JOURNAL OF SOLID STATE CHEMISTRY **131,** 252–262 (1997)
ARTICLE NO. SC977372

Preparation, Characterization, and *ab initio* X-Ray Powder Diffraction Study of $Cu_2(OH)_3(CH_3COO)\cdot H_2O$

Norberto Masciocchi,*[,1] Eleonora Corradi,* Angelo Sironi,* Giuliano Moretti,†[,1] Giuliano Minelli,† and Piero Porta†

*Dipartimento di Chimica Strutturale e Stereochimica Inorganica, Università di Milano, 20133 Milan, Italy; and †Centro del CNR ''SACSO,'' Dipartimento di Chimica, Università ''La Sapienza,'' 00185 Rome, Italy

Received November 15, 1996; accepted March 3, 1997

$Cu_2(OH)_3(CH_3COO)\cdot H_2O$ can be prepared by slow titration of 0.1 *M* copper acetate solution with NaOH 0.1 *M* to a OH^-/Cu^{2+} ratio of 1 or by heating at $50 < T < 75$°C copper acetate solutions with concentrations in the range $0.01\ M \leq [Cu^{2+}]_T \leq 0.18\ M$. This species has been characterized by *ab initio* XRPD structure determination, magnetic susceptibility measurements, and spectroscopic (XPS–XAES, FTIR) and thermal analyses. Crystals of $Cu_2(OH)_3(CH_3COO)\cdot H_2O$ are monoclinic, $P2_1/m$, $a=5.6025(5)$, $b=6.1120(6)$, $c=18.747(3)$ Å and $\beta=91.012(9)^\circ$, $Z=4$. $Cu_2(OH)_3(CH_3COO)\cdot H_2O$ is a structural analogue of the layered mineral botallackite; however, hydrogen bonded water molecules, which can be easily and reversibly removed by moderate heating, are intercalated between $Cu_2(OH)_3(CH_3COO)$ sheets. © 1997 Academic Press

INTRODUCTION

$Cu_2(OH)_3(CH_3COO)\cdot H_2O$ has been recently synthesized and characterized by a number of groups (1–3); on the basis of *very preliminary* diffraction data, it was suggested to possess a layer structure of the botallackite type, with easily exchangeable acetate ions, leading to topotactic and, in a few cases, reversible reactions (2, 3) if exposed to NO_3^-, ClO_4^-, Cl^-, Br^-, I^-, MnO_4^-, or SO_4^{2-} solutions. Like many other intractable polymeric complexes, $Cu_2(OH)_3(CH_3COO)\cdot H_2O$, which can only be obtained as a microcrystalline material, lacks, so far, a reliable structural characterization. Since we have recently studied the polymeric forms of $[Ru(CO)_4]$ (4), $[MX_2(\text{pyridazine})]$ (M = Mn, Fe, Co, Ni, Cu; X = Cl, Br) (5), $[MX_2(\text{4,4′-bipyridyl})]$ (M = Ni, Cu; X = Cl, Br) (6), Cu and Ag pyrazolates (7), and imidazolates (8), the crystal structures of which were successfully solved, and later refined, from standard laboratory X-ray powder diffraction data, we decided to tackle a complete structure determination, from powder diffraction data *only*, of the $Cu_2(OH)_3(CH_3COO)\cdot H_2O$ phase, the relevant results being reported in the following.

Our interest in $Cu_2(OH)_3(CH_3COO)\cdot H_2O$ was motivated by the preparative procedures of Cu–ZSM-5 catalysts for which a great number of papers have been published in recent years. These catalysts (differing in the Si/Al atomic ratios and copper loadings) are of interest as substitutes of the three-way catalysts based on noble metals (Pt, Rh, Pd) for removing NO_x, CO and HC from *lean* automobile exhaust (9, 10). In general, Cu–ZSM-5 catalysts are prepared by ion exchange of the zeolite with Cu^{2+} solutions (nitrate, sulphate, acetate, etc.). The best catalysts are the so-called *over-exchanged* Cu–ZSM-5 catalysts for which the copper loading is greater than the value permitted by the amount of aluminum in the ZSM-5 framework (1 mol Cu^{2+} exchanged per 2 mol Al^{3+}); they are normally prepared by adding NaOH or NH_3 (9) to warm (20–80°C) 0.01–0.1 *M* copper acetate solutions. During such a preparation, the precipitation of $Cu_2(OH)_3(CH_3COO)\cdot H_2O$ should be avoided because it easily transforms into CuO, with substantial loss of surface area and micropore volume of the catalysts (10, 11). Therefore, we have undertaken studies on the precipitation of $Cu_2(OH)_3(CH_3COO)\cdot H_2O$, under the influence of pH, total copper concentration, and temperature, and, in this paper, we report on its full physicochemical characterization by XRPD, XPS–XAES, magnetic susceptibility, FTIR, and TG-DTA analyses, thus extending previous work by Jiménez–Lòpez *et al.* (1) and by Yamanaka *et al.* [2].

EXPERIMENTAL

Preparation

The new preparation procedure of $Cu_2(OH)_3(CH_3COO)\cdot H_2O$ involves heating between 50 and 75°C of aqueous copper acetate solutions with concentrations in the range 0.01–0.18 *M*. A few samples were also prepared at room temperature using the standard procedure (1, 2) by slow titration of 0.1 *M* copper acetate solution with NaOH

[1] To whom correspondence should be addressed.

0022-4596/97 $25.00

0.1 *M* to an OH^-/Cu^{2+} ratio of 1. The precipitate in both cases was bluish-green. The copper content was determined by atomic absorption (Varian SpectrAA-30). C and H were determined by microanalysis by the staff of the Microanalytical Laboratory of the University of Milan. (Found: Cu = 48.8%, C = 9.50%, H = 2.95%. $Cu_2(OH)_3(CH_3COO)\cdot H_2O$ requires Cu = 49.8%, C = 9.41, H = 3.14%.)

Physical Measurements

X-ray photoelectron and X-ray excited Auger spectra (XPS–XAES) were obtained using Mg$K\alpha$ radiation ($h\nu = 1253.6$ eV) with a Leybold–Heraeus LHS-10 spectrometer operating at constant transmission energy ($E_0 =$ 50 eV) (1 eV $\approx 1.602 \times 10^{-19}$ J). The spectra were recorded at room temperature and with the X-ray generator operated at 12 kV and 20 mA. The vacuum in the analysis chamber was better than 10^{-8} mbar. Acquisition times of 3, 30, and 110 min were employed to check the possible decomposition of the basic copper acetate under X-ray illumination. The surface compositions of samples were obtained on the basis of the peak area intensities using the sensitivity factor method (12). The Fermi level of the sample was determined using the binding energy values of C(1s) of adventitious carbon (and of the methyl group of the acetate) fixed at 284.8 eV.

Magnetic susceptibility measurements were carried out on a Gouy balance in the range 90–300 K using a magnetic field of 0.8 T. The instrument was first calibrated with $Co[Hg(SCN)_4]$. The magnetic susceptibility was corrected only for the diamagnetism of the quartz tube. From the $1/\chi_m$ vs T plot, the values of the Weiss temperature, θ, and of the Curie constant, $C = \chi_m (T + \theta)$, were obtained.

The thermogravimetric curves were recorded with a Perkin–Elmer TGA7 instrument coupled with System 2000 FTIR spectrometer under nitrogen flux, at the heating rate of 20°C/min. This configuration allows the IR analysis of the gas which evolved during the thermal decomposition of the sample.

The IR spectra were recorded at room temperature from 4000 to 600 cm^{-1} on a Perkin–Elmer Paragon 1000 Spectrometer on nujol mulls (64 scans with a resolution of 2 cm^{-1}). KBr pellets proved to react with the title compound, possibly leading to substitution of the acetate groups by bromide ions.

The thermal behavior of the basic copper acetate in air was followed with a Stanton Redcroft STA 781 simultaneous TG–DTA apparatus (Pt crucibles, Pt–Pt–Rh thermocouples, heating rate 2–10°C/min). Typically, sample weights of 10–15 mg were employed during the runs. DSC measurements (Perkin–Elmer DSC 7 instrument, heating rate 10°C/min) of $Cu_2(OH)_3(CH_3COO)\cdot H_2O$ showed an endothermic peak at about 133°C (onset at about 106°C), while TG–DTA showed a weight loss of about 7.2% and an endothermic peak at ca. 125°C.

X-Ray Powder Diffractometry

The bluish-green powders were gently ground in an agate mortar and then cautiously deposited in the hollow of an aluminium sample holder, with the side loading technique (13), which is known to minimize preferred orientation effects in the plane normal to the scattering vector.

Initially, the diffraction data (run 1) were collected in the 5–105° (2θ) range, in θ–2θ mode and step scanning technique, with $\Delta 2\theta = 0.02°$ and counting time = 12 s on a Rigaku D/MAX III horizontal scan diffractometer (40 kV; 40 mA; Cu$K\alpha$ radiation). X-ray optics included parallel (Soller) slits and a curved graphite monochromator in the diffracted beam. Slits used were divergence 1.0°, antiscatter 1.0°, and receiving 0.3°.

Standard peak search methods were used to locate the diffraction maxima. TREOR (14) succeeded in finding a unit cell with approximate lattice constants of $a = 5.595$, $b =$ 6.109, $c = 18.697$ Å, $\beta = 91.75°$, $M(20) = 18$ (15), $F(20) = 34$ (0.013, 49) (16). A small peak at $d = 15.67$, of irreproducible intensity but observed also by the authors of Ref. (1), went unindexed and can be tentatively attributed to stacking faults, nonstoichiometric water spacers (*vide infra*), or partially carbonated layers (1). Systematic absences (0k0 $k = 2n$, and *dubious* $h0l$ $h = 2n$ conditions) indicated $P2_1/a$ or $P2_1/m$ as probable space groups; "structure solution" was possible in both cases, leading to the same basic structural motif of hexagonal Cu_nO_{2n} layers (but different acetate orientations). However, the dubious nature of the $h0l$ $h = 2n$ condition, crystal packing considerations, and existent stereochemical knowledge of such systems indicated $P2_1/m$ as the true space group. ALLHKL (17) was used to extract 220 integrated intensities in the 5–65° (2θ) range; direct methods (SIRPOW (18)) succeeded in locating three independent copper atoms, two of which lie on mirror planes; completion of the structural model was only possible by a tedious series of refinements and difference Fourier maps (using GSAS (19)).

Moreover, the diffraction peaks are fairly broad (FWHM $> 0.25°$, the nominal resolution for the present experimental setup being 0.12° for the NIST standard LaB_6) and some possess asymmetric tails in the high-angle side, indicating a probable faulted nature of the sample. In fact, as later discussed, the layered structure of $Cu_2(OH)_3(CH_3COO)\cdot H_2O$ can afford stacking faults and polytypes (such as those found in $Mg(OH)_2$, brucite, and brucite-related double-layer structures, i.e., brucitites (20)), together with acetate ligands disordered upon different lattice sites. Therefore, the fuzzy nature of the "swinging" acetate groups can be interpreted on the basis of such a model; indeed, the perchlorate

and hydroxyl ions in $Cu_7(OH)_{12}(ClO_4)_2$ are reported to be rather disordered (2, 21), and difficulties in locating the terminal oxygen atoms of the *ordered* nitrate in $Cu_2(OH)_3(NO_3)$ from XRPD data have also been encountered (22).

In order to remove the strong texture effects from our data, we performed several measurements on differently prepared samples, obtained by mixing the powders with silicon grease, arabic gum, wheat flour, or a fast hardening cyanoacrylate glue, later crushed into powders. All these methods removed, at least in part, preferred orientation effects but contained a high and partially structured background (fluorescence and/or amorphous halo of the matrix), which resulted in *artificially low* profile agreement factors (down to $R_p = 0.04$ and $R_{wp} = 0.06$!).

A further measurement (run 2) was made on a sample loaded in a spinning capillary glass tube and collected, in the Debye–Scherrer mode, on a Stoe diffractometer, equipped with Cu$K\alpha$ radiation source and a linear position sensitive detector (10° (2θ) wide) with step scans of 0.5° (2θ) in about 12 h [2–85° (2θ) range]; this specific mounting and the presence of a graphite monochromator in an incident beam were found to limit preferred orientation and specimen fluorescence effects, respectively. The final refinement was therefore completed on data set 2, by imposing chemical restraints (i) on the acetate groups and (ii) on the Cu–O distances of the CuO_6 octahedra (taken from Eby and Hawthorne (23), i.e., 1.97 Å for the short Cu–O distances and 2.40 Å for the Jahn–Teller elongated Cu ⋯ OH and Cu ⋯ $OCOCH_3$ distances). In the final model, the acetate residues possess 50 : 50 disordered methyl and oxo fragments, related to each other by the mirror plane bisecting the CH_3–C=O angle. A summary of crystal data and final fractional atomic coordinates are found in Tables 1 and 2, respectively. Figure 1 contains the observed and calculated powder patterns.

TABLE 1
Summary of Crystal Data and Structural Analysis for $Cu_2(OH)_3(CH_3COO)\cdot H_2O$

Formula	$C_2H_8Cu_2O_6$
fw (g mol^{-1})	255.16
Crystal system	Monoclinic
Space group	$P2_1/m$
a (Å)	5.6025(5)
b (Å)	6.1120(6)
c (Å)	18.747(3)
β (°)	91.012(9)
V (Å^3)	641.5(1)
ρ_{calc} (g cm^{-3})	2.642
μ_{calc} (cm^{-1})	152.3
$F(000)$	504
N_{obs}	3850
N_{refl}	1054
2θ range (°)	8–85
N_{par}	51
$N_{restraints}$	29
R_p[a]	0.18
R_{wp}	0.23
R_F	0.15

[a] $R_p = \sum|y_i - y_{ci}|/\sum y_i$, $R_{wp} = [\sum w_i(y_i - y_{ci})^2/\sum w_i y_i^2]^{1/2}$, $R_F = \sum|F_o - F_c|/\sum F_o$, where y_i and y_{ci} are the observed and calculated intensities at the ith step, respectively, w_i is a weighting factor (taken as $w_i = 1/y_i$), and F_o and F_c are observed and calculated structure factors for all the allowed reflections.

TABLE 2
Fractional Atomic Coordinates for $Cu_2(OH)_3(CH_3COO)\cdot H_2O$ (e.s.d.'s in Parentheses)

Atom	x/a	y/b	z/c
Cu1	0.1635(27)	0.0065(25)	0.2473(6)
Cu2	0.6662(33)	0.25	0.2688(9)
Cu3	0.6609(38)	− 0.25	0.2328(9)
O1	0.2657(31)	0.25	0.3102(11)
O2	0.2994(35)	− 0.25	0.2978(14)
O3	− 0.2132(23)	− 0.0355(14)	0.3029(9)
O4	0.0076(31)	0.25	0.1950(12)
O5	0.0603(34)	− 0.25	0.1905(13)
O6	0.5497(23)	0.0366(15)	0.1969(9)
C1	0.168(13)	0.25	0.3808(19)
C2[a]	0.117(8)	0.04459(12)	0.4159(13)
C3	− 0.040(10)	− 0.25	0.1182(16)
C4[a]	− 0.098(9)	− 0.04459(12)	0.0829(16)
Ow1	0.3032(107)	0.25	0.0509(27)
Ow2	− 0.4321(91)	0.25	0.4839(31)

[a] Disordered methyl and oxo groups (see Experimental).

The structural complexity, together with the quality of the powder patterns in our hands, which are definitely affected by a rather poor crystallinity and unavoidable texture, did not lead to a perfect match, the discrepancies between the observed data and calculated ones could not be fully eliminated. Therefore, in the following, we will rely mostly on the heavy atom location and coordination topology, rather than describing in detail the nature of the bonding and the expected anisotropy (for Jahn–Teller distortion) of the copper atoms environments. Despite the rather poor agreement factors, when dealing with such complex, poorly crystalline materials, more than ever, it is the visual inspection of the pattern matching and of the chemical soundness of the presented model which guarantee the correctness of the results.

RESULTS AND DISCUSSION

Preparation

In Fig. 2 we present the information useful to prepare $Cu_2(OH)_3(CH_3COO)\cdot H_2O$ by heating copper acetate solutions. It is there shown that the formation of $Cu_2(OH)_3$

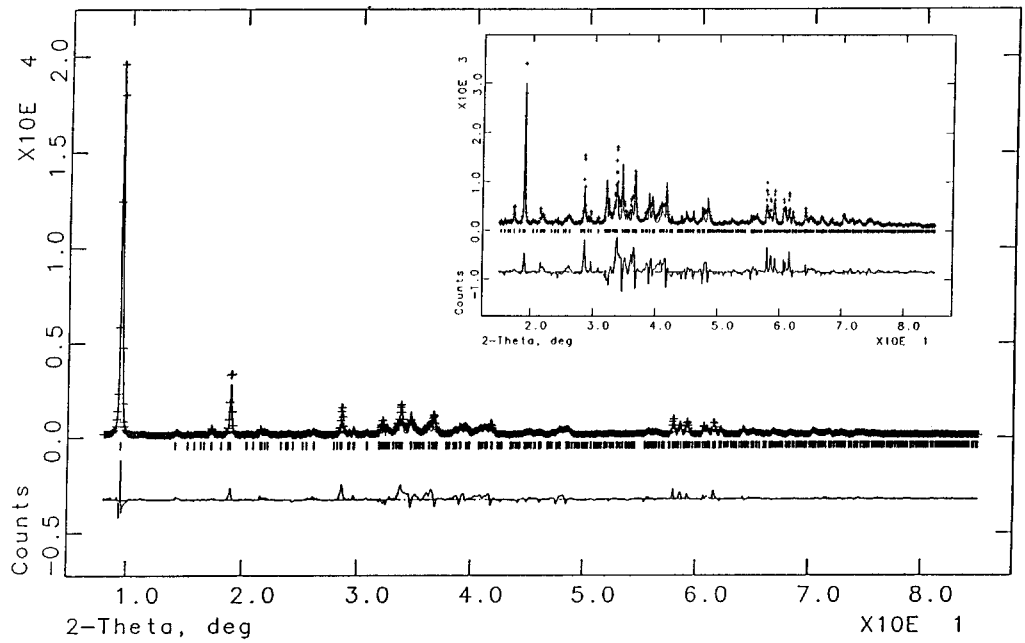

FIG. 1. Plot of the final Rietveld refinement for $Cu_2(OH)_3(CH_3COO)\cdot H_2O$, in the $8 < 2\theta < 85°$ range. Peak markers and difference plot are at the bottom. The inset shows the expansion of the high-angle data.

$(CH_3COO)\cdot H_2O$ occurs in the temperature range $50 < T < 75°C$ and in the concentration range $0.01\ M \leq [Cu^{2+}]_T \leq 0.18\ M$ (with pH values always lying in the $5 <$ pH < 6 range). For concentrations below 0.01 *M* no precipitation occurs. At $T = 80°C$ we note the formation of a dark-brown precipitate, probably CuO, due to the decomposition of amorphous $Cu(OH)_2$. This is in agreement with the results of Candal *et al.* (24). These authors reported the formation of CuO by decomposing at 70–80°C amorphous $Cu(OH)_2$ from dilute copper solutions ($[Cu^{2+}]_T \leq 0.01\ M$) at pH ≈ 6.

Figure 3 shows the pH of a copper acetate solution, initially 0.36 *M*, at 70°C as a function of the water added to the solution. We see that for concentrations lower than 0.18 *M* the precipitation of $Cu_2(OH)_3(CH_3COO)\cdot H_2O$ occurs with pH between 5.6 and 5.8.

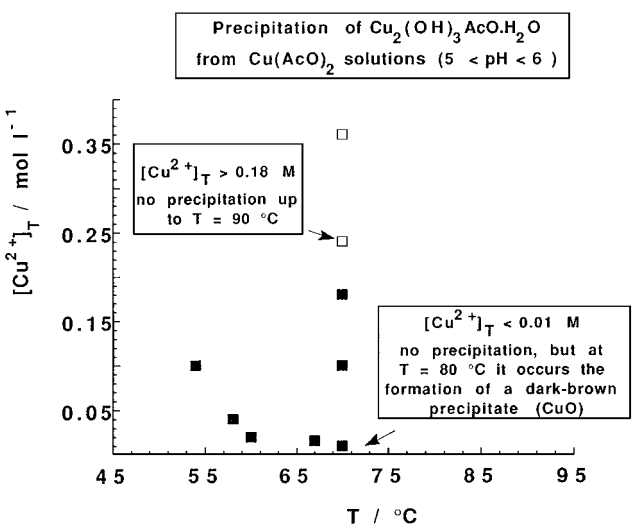

FIG. 2. Conditions of concentration and temperature for the precipitation of $Cu_2(OH)_3(CH_3COO)\cdot H_2O$ from copper acetate solutions (solid symbols: precipitate; open symbols: clear solution).

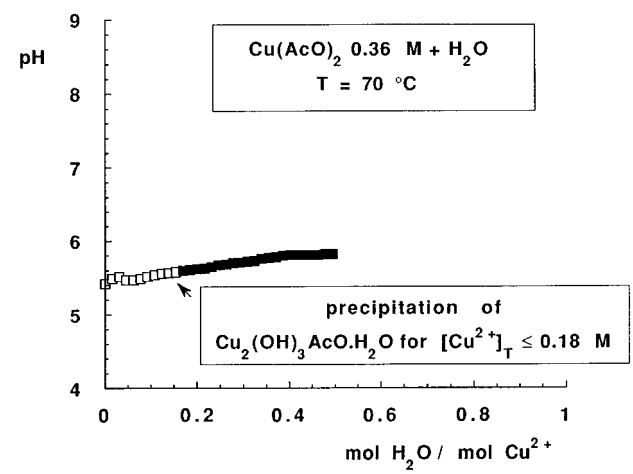

FIG. 3. Dilution of a copper acetate solution 0.36 *M* with water at 70°C.

The method normally employed in the preparation of $Cu_2(OH)_3(CH_3COO)\cdot H_2O$ requires the addition of NaOH at room temperature up to a OH^-/Cu^{2+} ratio of 1 (1, 2). With copper acetate solutions 0.02 and 0.10 *M* the pH of the solution in equilibrium with the solid, at $OH^-/Cu^{2+} = 1$, is about 5.8, in agreement with our observation that copper acetate solutions 0.01–0.18 *M*, heated in the range $50 < T < 75$°C, lead to the formation of $Cu_2(OH)_3(CH_3COO)\cdot H_2O$ with a pH always lying between 5 and 6.

Crystal Chemistry

The Cu(II) hydroxo-salt $Cu_2(OH)_3(CH_3COO)\cdot H_2O$ is structurally related to the mineral botallackite $Cu_2(OH)_3Cl$ (25) and its congeners, such as $Cu_2(OH)_3Br$ (26), $Cu_2(OH)_3I$ (27), and $Cu_2(OH)_3(NO_3)$ (22, 28); these known species, however, do not contain water molecules hosted in the crystal lattice. The structural relation among these phases, is readily evidenced by the synoptic collection of Table 3, where lattice constants and space group symmetries are compared.

All compounds listed in Table 3 are based on $Cu_2(OH)_3X$ layers, each containing hexagonally packed copper atoms bridges in a regular fashion by μ_3-OH or μ_3-*X* anions, stacked along the *c* axis. The similarity of lattice constants in the *ab* plane reveals the absence of "crystallochemical shifts" induced by the different nature of the anions. However, the different sizes of the X^- ligands are clearly reflected by the continuous increase of the *c* axis on passing from chloride to bromide, iodide, and nitrate. On the basis of rough volume estimates for the acetate group, a *c* value for a crystal isomorphous to the corresponding halides could be guessed to lie in the 7.2–7.5 Å range; the measured value of 18.67 (i.e., 2×9.33) Å, therefore, must be a manifestation of (i) a new structural pattern based on the stacking of a couple of layers and (ii) the presence of water molecules hosted in the crystal lattice (see Experimental). Consistently, when $Cu_2(OH)_3(CH_3COO)\cdot H_2O$ is heated for a few minutes at 140°C, water is lost and the new crystalline phase $[Cu_2(OH)_3(CH_3COO)]$ is generated. The XRPD pattern of the latter, collected under nitrogen atmosphere, shows intense peaks at 2θ 12.23 and 24.46°, corresponding to an interlayer spacing of 7.22 Å (the overall spectrum being indexed by a monoclinic cell with $a = 5.59$, $b = 13.00$, $c = 14.44$ Å, and $\beta = 91.8$°). On exposing the sample to aerial humidity, the starting $Cu_2(OH)_3(CH_3COO)\cdot H_2O$ phase is rapidly restored. The kinetics of such a transformation have been followed by XRPD (fast scans in the 8 to 14° (2θ) range of a freshly prepared dehydrated sample left in air). For a temperature of 20°C and a relative humidity of 45% ($p(H_2O) = 7.9$ Torr), the original hydrated phase is completely restored after 3 h (Fig. 4); on analyzing this time dependence by the 13 kinetic models reported by Byrn (29), only the Avrami–Erofeev equation (30) (with $n = 0.25$) leads to a satisfactory fitting of our kinetic data (correlation coefficient > 0.997), thus suggesting that the rehydration process is governed by three-dimensional random nucleation.

The final refined structure (see Fig. 5) shows that the $Cu_2(OH)_3(CH_3COO)$ layers stack above each other by inversion centers; within each layer, the acetato groups lie alternatively on both sides. Note that in the initially guessed (see Experimental) $P2_1/a$ space group they were bound to lie on the very same side of each layer (with very short, unplausible, packing contacts); this would have been rather surprising, since in all other compounds reported in Table 3, the *X* ions are orderedly arranged on both sides of each layer. Given the rather large size of the CH_3COO^- ligand (if compared to halides or nitrate), water molecules, hydrogen bonded to hydroxyl, and/or carbonyl groups are necessary both to fill the incipient cavities and to avoid short interlayer C–H ⋯ H–C contacts.

In the crystal structure of pristine $Cu_2(OH)_3(CH_3COO)\cdot H_2O$, the copper atoms of neighboring layers are not superimposable when projected down [001]; therefore, the observed doubling of the *c* axis is a mere consequence of the structural relation among these layers, which are related to each other by inversion centers, rather than by simple lattice translations.

TABLE 3
Synoptic Collection of Lattice Metrics and Symmetries for $Cu_2(OH)_3(CH_3COO)\cdot H_2O$ and Its Congeners

Compound	*a*	*b*	*c*	α	β	γ	Space group	Ref.
$Cu_2(OH)_3Cl$	5.63	6.12	5.73	90	93.4	90	$P2_1/m$	(25)
$Cu_2(OH)_3Br$	5.64	6.14	6.06	90	93.3	90	$P2_1/m$	(26)
$Cu_2(OH)_3I$	5.65	6.16	6.56	90	95.2	90	$P2_1/m$	(27)
$Cu_2(OH)_3(NO_3)$,[a] R.T.	5.60	6.08	6.93	90	94.6	90	$P2_1$	(28)
$Cu_2(OH)_3(NO_3)$, High T.	5.61	6.10	6.98	90	92.4	90	$P2_1$	(22)
$Cu_2(OH)_3(CH_3COO)\cdot H_2O$	5.60	6.10	18.70	90	92.0	90	$P2_1/m$	This work
$Cu_2(OH)_3(CH_3COO)$	5.59	13.00	14.44	90	91.8	90	Monoclinic *P*	This work

[a] A slightly different structure, differing in the $-NO_3$ orientation, was originally formulated (Ref. (28a)) in space group $P2_1/m$.

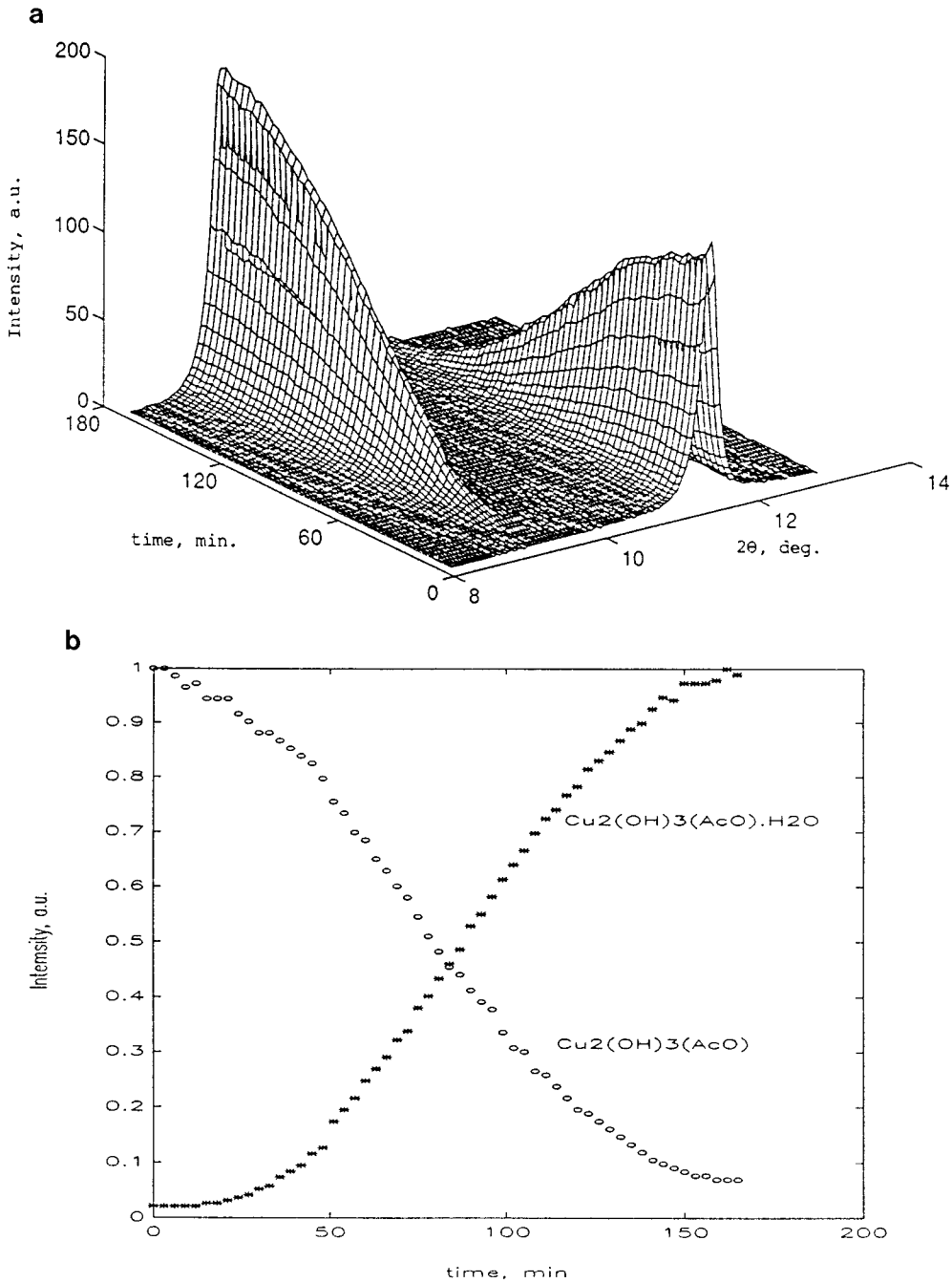

FIG. 4. Time evolution of a XRPD spectrum for open air rehydration of the $Cu_2(OH)_3(CH_3COO)$ phase: (a) raw data in the $8 < 2\theta < 14^\circ$ range; (b) evolution of the (normalized) peak heights vs time (note that a partial hysteresis is present at the beginning of the transformation, as evidenced by the marked "hook" effect at low reaction times).

XPS–XAES

The binding energies of the C(1*s*), O(1*s*), Cu($2p_{3/2}$) photoemission peaks, as well as the Cu($L_3M_{45}M_{45}$, ^1G) Auger kinetic energy, are reported in Table 4. The full widths at half maximum of O(1*s*) and Cu($2p_{3/2}$) transitions increase as a function of the acquisition time pointing to a partial reduction of Cu^{2+} species (31) and loss of interlayer water molecules.

The $-COO^-/Cu^{2+}$ atomic ratio, obtained from the intensity ratios using the sensitivity factor approach (12), is in good agreement (within the 20% error, intrinsic in the

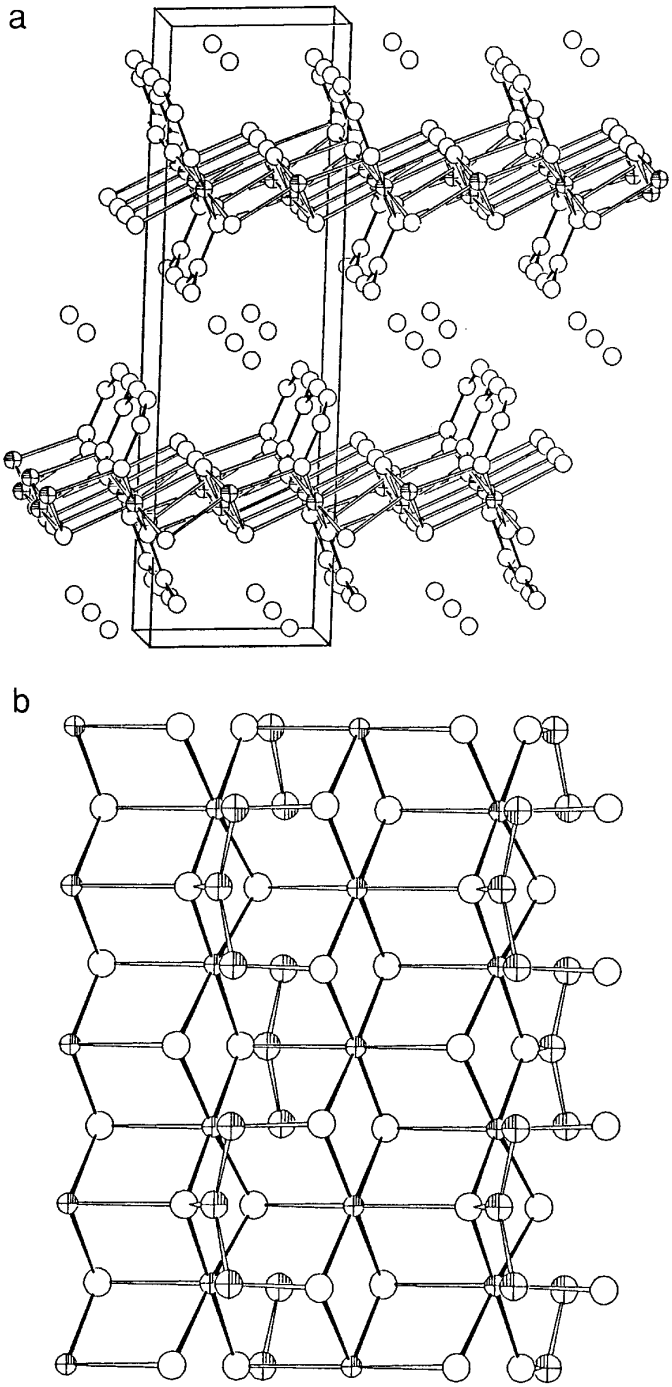

FIG. 5. Schematic plot of the crystal structure (a) of $Cu_2(OH)_3(CH_3COO)\cdot H_2O$ viewed approximately down [010], showing the stacking, along *c*, of the $Cu_2(OH)_3(CH_3COO)$ layers (b) and intercalated water molecules (empty circles). Relevant distances: Cu1 ··· Cu1′ 3.13(3), Cu1 ··· Cu1″ 2.98(3), Cu1 ··· Cu2 3.20(3), Cu1 ··· Cu2* 3.20(3), Cu1 ··· Cu3 3.22(3), Cu1 ··· Cu3* 3.23(3), Cu2 ··· Cu3 3.129(4) Å. Symmetry operators: ′*x*, 1/2 − *y*, *z*; ″*x*, −1/2 − *y*, *z*; *1 − *x*, *y*, *z*.

TABLE 4
XPS–XAES Data for $Cu_2(OH)_3(CH_3COO)\cdot H_2O$ Obtained with 110 min of X-Ray Irradiation

Transition	E_b(eV)	E_k(eV)
Cu ($2p_{3/2}$)	934.5 (4.5–110 min) (4.0–30 min) (3.8–3 min)	
O(1*s*)	531.3 (2.7–110 min) (2.4–30 min)	
C(1*s*)	284.8 ($-CH_3$ "C") (2.3–110 min) 288.2 ($-COO^-$) (2.3–110 min)	
$Cu(L_3M_{45}M_{45}, {}^1G)$		916.7
Atomic ratios	Calculated for $Cu_2(OH)_3(CH_3COO)$	Measured (surface)
C(−COO)/Cu	0.50	0.42
O/Cu	2.5	1.92

Note. Using the contamination carbon as a reference (aliphatic carbon with the binding energy of C(1*s*) fixed at 284.8 eV) the charging of the sample was +6.7 eV. In parentheses, the full width at half maximum (FWHM) of the XPS peaks. FWHM are also reported for Cu($2p_{3/2}$) and O(1s) for shorter acquisition times. Sensitivity factors were taken from Ref. (12).

method) with the value calculated from the formula (Table 4). The O/Cu atomic ratio is also in agreement considering the loss of interlayer water molecules. Figure 6 shows the Cu($2p_{3/2}$) transitions peaks for $Cu_2(OH)_3(CH_3COO)\cdot H_2O$ (3 min under X rays), CuO, $Cu_2(OH)_2CO_3$, and $CuAl_2O_4$ (31, 32). One can see that the general aspect of the spectrum is similar for all these compounds. The Cu($2p_{3/2}$) peak is characterized by a main peak, at lower binding energy, which originates from the well-screened final state $2p^53d^{10}\underline{L}$, where $\underline{L}$ denotes a hole on an oxygen atom. At higher binding energies, a satellite peak, related to a poorly screened state, is present, the character of which is $2p^53d^9$. The energy separation and the relative intensity of the satellite peak depend on the hybridization between the copper 3*d* and the oxygen 2*p* states (33). On increasing the covalency of the Cu–O chemical bond, the separation between the satellite and the main peaks (Δ) is raised and the relative intensity of the satellite peak (I_s/I_m) lowered (34). From Fig. 6, it can be seen that the energy separation decreases in the order $CuO > Cu_2(OH)_3(CH_3COO)\cdot H_2O > CuAl_2O_4 > Cu_2(OH)_2CO_3$. The intensity ratio between the satellite and the main peak (after smoothing of the data and subtraction of a linear background) follows the inverse order, i.e., $Cu_2(OH)_2CO_3 > CuAl_2O_4 > Cu_2(OH)_3(CH_3COO)\cdot H_2O > CuO$. Note that this order gives the relative scale of ionicity of the Cu–O chemical bond. It appears, therefore, that the ionicity of the

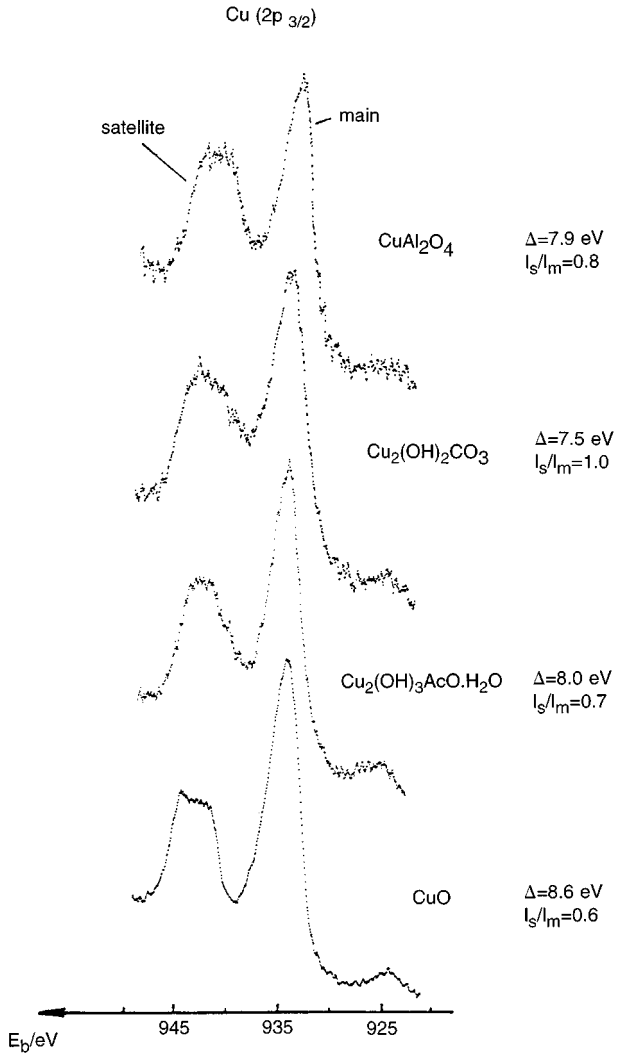

FIG. 6. Cu($2p_{3/2}$) transition in $Cu_2(OH)_3(CH_3COO)\cdot H_2O$ and for comparison in CuO, $CuAl_2O_4$ and $Cu_2(OH)_2CO_3$. The separation between the satellite peak and the main peak (Δ) and the relative intensity ratio (I_s/I_m) are also reported.

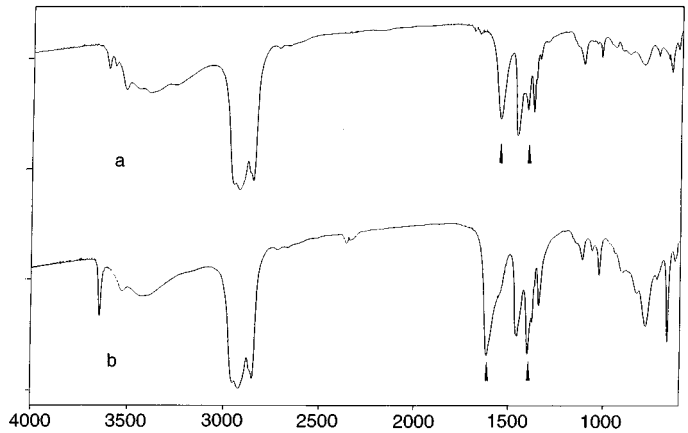

FIG. 7. Infrared spectra (nujol mulls; transmittance vs wavenumbers [cm^{-1}]) of $Cu_2(OH)_3(CH_3COO)\cdot H_2O$ (a) and $Cu_2(OH)_3(CH_3COO)$ (b); arrowheads indicate $\nu(-COO^-)$ stretching modes.

Cu–O bonds in $Cu_2(OH)_3(CH_3COO)\cdot H_2O$ is intermediate between that of copper aluminate and copper oxide.

FTIR

The IR spectrum of $Cu_2(OH)_3(CH_3COO)\cdot H_2O$, similar to what has been reported by Jiménez–Lòpez *et al.* [1], shows two intense bands at 1550 and 1410 cm^{-1}, assigned to $\nu_{as}(-COO^-)$ and $\nu_s(-COO^-)$, respectively (see Fig. 7a). The difference between these two frequencies is characteristic of a bridging acetate ligand (μ_3-$OCOCH_3$ fragments are rare (35) and uncharacterized from a vibrational point of view). The proposed structural model contains the acetate fragment bound to the copper atoms via a single oxygen atom and should therefore afford $\nu(-COO^-)$ absorption frequencies separated by at least 200 cm^{-1} (36); however, the presence of a neighboring hydroxyl, capable of binding, via hydrogen bonding, the "free" >C=O moiety, lowers the difference between the two modes by generating a "μ_4–η_2-bridging" acetate group as in Scheme 1a.

Interestingly, in the pseudoisomorphous anhydrous phase, the *b* axis (beside being doubled) slightly expands, raising the (probable) C=O ··· H value to 3.25 Å or more (see Table 3); consistently, although in the absence of a suitable structural model, the two bands differ by more than 200 cm^{-1} in the IR spectrum of $Cu_2(OH)_3(CH_3COO)$, suggesting a loss of hydrogen bonds between the "bridging" acetate and the neighboring hydroxyls [$\nu_{as}(-COO^-) =$ 1618 and $\nu_s(-COO^-)$ 1400 cm^{-1}; see Scheme 1b and Fig. 7b].

Five discernible maxima are present in the OH stretching vibrations of $Cu_2(OH)_3(CH_3COO)\cdot H_2O$ (3613, 3563, 3529, 3410, and 3275 cm^{-1}). The sharp bands at 3613 and

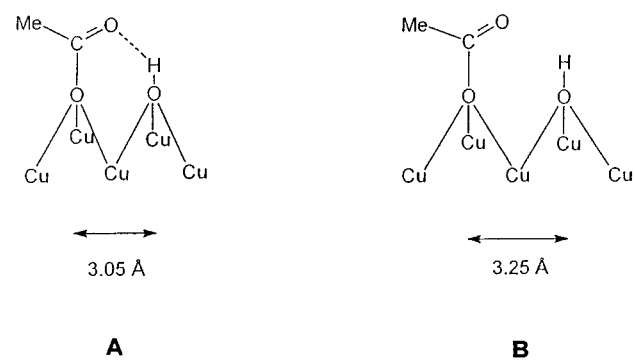

SCHEME 1

3563 cm^{-1} are assigned to stretching vibration of OH groups *not* involved in hydrogen bonding, whereas the medium intensity broader bands are assigned to weakly interacting hydroxyls and/or interlayer water. Upon dehydration, only one (very) sharp OH stretching vibration (3647 cm^{-1}) and two broad bands (3531 and 3427 cm^{-1}) are observed.

TG–DTA–DSC and FTIR–TG

Figure 8 shows the TG–DTA traces obtained in air with a heating rate of 2°C/min. We found that it is very important to employ very low heating rates because the last step in the decomposition is fast and very esothermic. At 10°C/min the total loss is larger than expected, probably due to mechanical ablation of the sample caused by the tumultuous evolution of the gas(es).

The first peaks in the DTA and DSC curves (onset at 106°C) correspond to the loss of the water molecules of the interlayer region, with a measured ΔH value of 52.3 KJ mol^{-1} (for comparison, the heat of vaporization of pure water at 100°C is 40.7 KJ mol^{-1}):

$$Cu_2(OH)_3(CH_3COO)\cdot H_2O \rightarrow Cu_2(OH)_3(CH_3COO) + H_2O_{(g)}$$

(endothermic, up to ca. 125°C).

Further peaks, above 170°C, are poorly resolved and correspond to the complete thermal decomposition, which can be best represented by the following reactions:

$$Cu_2(OH)_3(CH_3COO) \rightarrow Cu_2O(OH)_2 + CH_3COOH$$

(endothermic, up to ca. 180°C)

$$Cu_2O(OH)_2 \rightarrow 2CuO + H_2O_{(g)}$$

(esothermic, up to ca. 220°C).

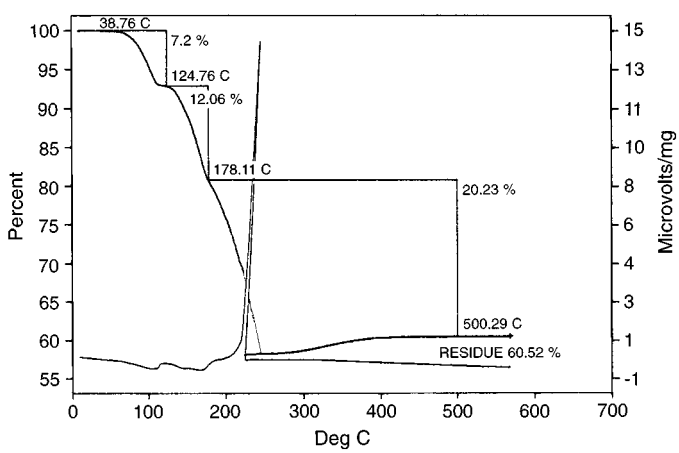

FIG. 8. TG (left ordinate) and DTA (right ordinate) of $Cu_2(OH)_3(CH_3COO)\cdot H_2O$ obtained in air with a heating rate of 2°C/min.

It should be noted, however, that the second and third steps partially overlap.

The IR spectra of the gas evolved during thermal analysis in N_2 (heating rate = 20°C/min) show that the loss of the acetic acid starts at about 160°C and continues up to 250°C. The endotherm in the DTA up to about 180°C confirms the departure of CH_3COOH rather than its decomposition, which should be recorded as an esotherm. Summarizing, the thermal analysis points out the low thermal stability of $Cu_2(OH)_3(CH_3COO)\cdot H_2O$.

If the DSC and TG–DTA analyses are performed on the samples of lower crystallinity (i.e., those possessing the high-*d* spacing in their XRPD patterns), a more complex picture is found, with a partial overlap of all aforementioned steps, and a more complex pattern of the first transition, where water is lost. Again, this could be related to the different nature of the sample, where a nonstoichiometric ratio of water is present.

Magnetic Susceptibility

The magnetic data are a sensitive probe of the interactions between the paramagnetic Cu^{2+} ions. On analyzing the susceptibility data by the Curie–Weiss law, in the 100–300 K range, a magnetic moment of ca. 1.9 μ_B and a Weiss constant $\theta = -7(1)$ K are obtained. Very recently, a number of magnetic studies of the title compound (37) and of structural analogues have been performed on oriented single crystals (38) or powders (39). The magnetic results for $Cu_2(OH)_3(CH_3COO)\cdot H_2O$ reported by Rabu *et al.* (37) indicate that at high temperatures (20–300 K) an antiferromagnetic interaction between the Cu^{2+} spins (μ_{Cu} ca. 1.9 μ_B) takes place; at 10 K, however, there is a slight increase in the atomic magnetic susceptibility (χ_{Cu}), suggesting a weak ferromagnetic *intra*layer interaction. Finally, at lower temperatures, a drop in χ_{Cu} indicates that *inter*layer interactions result in a three-dimensional ordered state. Our results in the range 100–300 K are also in good agreement with the data reported for $Cu_2(OH)_3(NO_3)$ [μ_{Cu} 1.75(1) μ_B and $\theta = -8(1)$] (38), indicating that the copper atoms are antiferromagnetically coupled. Unfortunately, the extensive magnetic study performed on the $Cu_2(OH)_3(n\text{-}C_mH_{2m+1}COO)$ species ($m = 0$, 1, 7, 8, and 9) lacks a detailed characterization of the $m = 1$ member (39).

CONCLUSIONS

Previously, it was reported that the precipitation of $Cu_2(OH)_3(CH_3COO)\cdot H_2O$ at room temperature is mediated by OH^- groups added to the solution of copper acetate [see Refs. (1, 2) and references therein]. A basic copper acetate containing 2 acetate and 2 OH^- groups was

also prepared adding urea to a 0.1 *M* copper acetate solution at 70°C (6 mol of urea per mol of Cu) (40). We have here demonstrated that spontaneous precipitation of $Cu_2(OH)_3$ $(CH_3COO)\cdot H_2O$ also occurs on heating the acetate solutions in the temperature range $50 < T < 75$°C for copper concentrations in the 0.01–0.18 *M* range. This effect is utmost importance in the preparation of over-exchanged Cu–ZSM-5 catalysts, where the copper loadings exceed the maximum amount permitted by the aluminium present in the framework of the ZSM-5 zeolite. The best over-exchanged catalysts are those where low-nuclearity copper species are exchanged before $Cu_2(OH)_3(CH_3COO)\cdot H_2O$ is formed; indeed, the precipitation of the basic copper acetate on the external surface and possibly at the intersection of the ZSM-5 zeolite channels leads, after its decomposition at high temperature, to CuO with consequent loss of surface area and porosity of the catalysts (10).

The presented work also reports on the crystal structure determination from powder diffraction data of a microcrystalline phase which could not be grown as single crystals of suitable quality. The efforts put into the experimental and structural analysis procedures are witnessed by the quality of the final XRPD pattern (raw data of data set 2) if compared to those collected on the extremely highly textured sample reported in Ref. (1). Although the structural characterization of anhydrous basic copper acetate is still incomplete and the refinement of the structural features of the hydrated phase is of poorer quality than those of several analogues characterized either on single-crystal or on powder diffraction data (see Table 3), the present study shows that it is possible to obtain useful structural data even from such complex patterns, where poor crystallinity, nonnegligible texture, and high fluorescence effects hide the theoretical (aberration-free) powder spectrum of an ideal sample. Note that, in the present case, *profile* agreement factors *alone* did not allow us to discriminate between the $P2_1/a$ and $P2_1/m$ models; it was only the fruitful combination of the previous knowledge of the structure of similar layered compounds and of the reversible topotactical behavior of anion exchange reactions, together with the above-mentioned stereochemical considerations, which eventually led to the final model presented in Tables 1 and 2 and in Fig. 5.

ACKNOWLEDGMENTS

We are indebted to Dr. Monica Bartolomei (Istituto Superiore di Sanità, Rome) for collecting the TG-FTIR data. We thank Dr. Maurizio Bellotto, University of Mulhouse, for helpful discussions and for assisting with the experimental work. The Italian CNR and MURST are acknowledged for funding.

REFERENCES

1. A. Jiménez-Lòpez, E. Rodriguez-Castellòn, P. Olivera-Pastor, P. Maireles-Torres, A. A. G. Tomlinson, D. J. Jones, and J. Rozière, *J. Mater. Chem.* **3,** 303 (1993).
2. S. Yamanaka, T. Sako, K. Seki, and M. Hattori, *Solid State Ionics* **53,** 527 (1992).
3. S. Yamanaka, T. Sako, and M. Hattori, *Chem. Lett*., 1869 (1989).
4. N. Masciocchi, M. Moret, P. Cairati, F. Ragaini, and A. Sironi, *J. Chem. Soc*., *Dalton Trans*., 471 (1993).
5. N. Masciocchi, P. Cairati, L. Carlucci, G. Ciani, G. Mezza, and A. Sironi, *J. Chem. Soc*., *Dalton Trans*., 3009 (1994).
6. N. Masciocchi, P. Cairati, L. Carlucci, G. Ciani, G. Mezza, and A. Sironi, *J. Chem. Soc*., *Dalton Trans*., 1351 (1996).
7. N. Masciocchi, M. Moret, P. Cairati, A. Sironi, G. A. Ardizzoia, and G. La Monica, *J. Am. Chem. Soc*. **116,** 7668 (1994).
8. N. Masciocchi, M. Moret, P. Cairati, A. Sironi, G. A. Ardizzoia, and G. La Monica, *J. Chem. Soc*., *Dalton Trans*., 1671 (1995).
9. M. Shelef, *Chem. Rev*., **95,** 209 (1995).
10. P. Ciambelli, P. Corbo, M. Gambino, F. Migliardini, G. Minelli, G. Moretti, and P. Porta, *in* "Zeolites: A Refined Tool for Designing Catalytic Sites (L. Bonneviot and S. Kaliaguine, Eds.), p. 295. Elsevier, Amsterdam, 1995; G. Moretti, G. Minelli, P. Porta, P. Ciambelli, P. Corbo, M. Gambino, F. Migliardini, and S. Iacoponi, *in* "Proceedings of the 11th International Zeolite Conference," Seoul, Korea, Aug. 12–17, 1996, Elsevier, Amsterdam, 1996.
11. J. N. Armor and T. S. Farris, *Appl. Catal. B*: *Environmental* **4,** L11 (1994).
12. C. D. Wagner, L. E. Davis, M. V. Zeller, J. A. Taylor, R. M. Raymond, and L. H. Gale, *Surf. Interface Anal.* **3,** 211 (1981).
13. H.F. McMurdie, M. Morris, E. Evans, B. Paretzkin, and W. Wong-Ng, *Powder Diffr*. **1,** 40 (1986).
14. P. E. Werner, L. Eriksson, and M. Westdahl, *J. Appl. Crytallogr*. **18,** 367 (1985).
15. P. M. De Wolff, *J. Appl. Crystallogr*. **1,** 108 (1968).
16. G. S. Smith and R. L. Snyder, *J. Appl. Crystallogr*. **12,** 60 (1979).
17. G. S. Pawley, *J. Appl. Crystallogr*. **14,** 357 (1981).
18. G. Cascarano, L. Favia and C. Giacovazzo, *J. Appl. Crystallogr*. **25,** 310 (1992).
19. A. C. Larson and R. B. Von Dreele [unpublished manuscript, LANSCE, Ms-H805, Los Alamos National Laboratory, New Mexico, 1990]
20. W. Hofmeister and H. von Platen, *Cryst. Rev*. **3,** 29 (1992).
21. R. Nasanen and V. Tamminen, *J. Am. Chem. Soc*. **71,** 1994 (1949).
22. N. Guillou, M. Louër, and D. Louër, *J. Sol. State Chem*. **109,** 307 (1994).
23. R. K. Eby and F. C. Hawthorne, *Acta Crystallogr. B* **49,** 28 (1993).
24. R. J. Candal, A. E. Regazzoni, and M. A. Blesa, *J. Mater. Chem*. **2,** 657 (1992).
25. A. A. Voronova and B. K. Vainshtein, *Krystallografija* **3,** 444 (1958).
26. F. Aebi, *Helv. Chim. Acta* **31,** 369 (1948).
27. H. R. Oswald and W. Feitknecht, *Helv. Chim. Acta* **47,** 272 (1964).
28. (a) W. Nowacki and R. Scheidegger, *Acta Crystallogr*. **3,** 472 (1950); *Helv. Chim. Acta* **35,** 375 (1952); (b) H. Effenberger, *Z. Kristallogr*. **165,** 127 (1983).
29. S. R. Byrn, "Solid-State Chemistry of Drugs," p. 60. Academic Press, New York, 1982.
30. M. Avrami, *J. Chem. Phys*. **9,** 177 (1941). [and references therein]
31. G. Moretti, G. Fierro, M. Lo Jacono, and P. Porta, *Surf. Interface Anal*. **14,** 325 (1989).
32. G. Moretti and P. Porta, *Surf. Interface Anal*. **15,** 47 (1990).

33. K. Okada, J. Kawai, and A. Kotani, *Phys. Rev. B* **48,** 10733 (1993).
34. G. van der Laan, C. Westra, C. Haas, and G. A. Sawatzky, *Phys. Rev. B* **23,** 4369 (1981).
35. G. Smith, E. J. O'Reilly, and C. H. L. Kennard, *Aust. J. Chem.* **34,** 891 (1981).
36. K. Nakamoto, "Infrared and Raman Spectra," p. 233. Wiley, New York, 1986.
37. P. Rabu, S. Rouba, V. Laget, C. Hornick, and M. Drillon, *J. Chem. Soc., Chem. Commun.*, 1107 (1996).
38. G.-G. Linder, M. Atanasov, and J. Pebler, *J. Solid State Chem.* **116,** 1 (1995).
39. W. Fujita and K. Awaga, *Inorg. Chem.* **35,** 1915 (1916).
40. S. M. Teler, S. A. Sadeek, and El. M. Nour, *J. Phys. Chem. Solids* **54,** 1993 (1993).